Cytosolic calcium accumulation and delayed repolarization associated with ventricular arrhythmias in a guinea pig model of Andersen-Tawil syndrome

Przemysław B. Radwański, PharmD,*† Rengasayee Veeraraghavan,*‡ Steven Poelzing, PhD*‡

*From the *Nora Eccles Harrison Cardiovascular Research and Training Institute, †Department of Pharmacology and Toxicology, and ‡Department of Bioengineering, University of Utah, Salt Lake City, Utah.*

BACKGROUND Andersen-Tawil syndrome (ATS1)–associated ventricular arrhythmias are initiated by frequent, hypokalemia-exacerbated, triggered activity. Previous *ex vivo* studies in drug-induced Andersen-Tawil syndrome (DI-ATS1) models have proposed that arrhythmia propensity in DI-ATS1 derives from cytosolic Ca^{2+} ($[Ca^{2+}]_i$) accumulation leading to increased triggered activity.

OBJECTIVE The purpose of this study was to test the hypothesis that elevated $[Ca^{2+}]_i$ with concomitant APD prolongation, rather than APD dispersion, underlies arrhythmia propensity during DI-ATS1.

METHODS DI-ATS1 was induced in isolated guinea pig ventricles by perfusion of 2 mM KCl Tyrode solution containing 10 μM $BaCl_2$. APD and $[Ca^{2+}]_i$ from the anterior epicardium were quantified by ratiometric optical voltage (di-4-ANEPPS) or Ca^{2+} (Indo-1) mapping during right ventricular pacing with or without the ATP-sensitive potassium channel opener pinacidil (15 μM).

RESULTS APD gradients under all conditions were insufficient for arrhythmia induction by programmed stimulation. However, 38% of DI-ATS1 preparations experienced ventricular tachycardias (VTs), and all preparations experienced a high incidence of premature ventricular complexes (PVCs). Pinacidil decreased APD and APD dispersion and reduced VTs (to 6%), and PVC frequency (by 79.5%). However, PVC frequency remained significantly greater relative to control (0.5% ± 0.3% of DI-ATS1). Importantly, increased arrhythmia propensity during DI-ATS1 was associated with diastolic $[Ca^{2+}]_i$ accumulation and increased $[Ca^{2+}]_i$ transient amplitudes. Pinacidil partially attenuated the former but did not alter the latter.

CONCLUSION The study data suggest that arrhythmias during DI-ATS1 may be a result of triggered activity secondary to prolonged APD and altered $[Ca^{2+}]_i$ cycling and less likely dependent on large epicardial APD gradients forming the substrate for reentry. Therefore, therapies aimed at reducing $[Ca^{2+}]_i$ rather than APD gradients may prove effective in treatment of ATS1.

KEYWORDS Arrhythmia mechanism; Cellular calcium; Mapping; Repolarization; Ventricular arrhythmia

ABBREVIATIONS APD = action potential duration; **APD$_{50}$** = 50% of action potential duration; **ATS1** = Anderson-Tawil syndrome; **BCL** = basic cycle length; **Ca^{2+}** = calcium; **[Ca^{2+}]$_i$** = cytosolic Ca^{2+}; **DI-ATS1** = drug-induced Anderson-Tawil syndrome; **ECG** = electrocardiogram; **F$_{405}$/F$_{485}$** = calculated ratiometric Ca^{2+} signal; **I$_{K1}$** = inward rectifier potassium current; **QTc** = corrected QT; **PVC** = premature ventricular complex; **VT** = ventricular tachycardia

Introduction

Anderson-Tawil syndrome (ATS1) is an inherited channelopathy that results from loss of function of the inward-rectifier K$^+$ current (I$_{K1}$) secondary to mutations in *KCNJ2*, the gene that encodes the Kir2.1 channel.[1,2] ATS1 is characterized electrocardiographically by a prolonged QT interval (hence its classification as long QT syndrome type 7) and nonsustained ventricular tachycardias (VTs) that often are foreshadowed by frequent triggered activity and occur more frequently during hypokalemia.[2,3] Therefore, it has been proposed that arrhythmias in ATS1 may be caused by electrical substrate remodeling[4,5] giving rise to the prolonged QT interval and increased triggered activity frequency. Although heterogeneous action potential duration (APD) prolongation and increased dispersion, both transmural and interventricular, have been reported in experimental models of ATS1,[5–7] whether these gradients of repolarization are sufficient for reentry to occur remains unknown.

The high frequency and focal nature of bidirectional VTs in ATS1 suggest that triggered activity underlies, at least in part, the observed arrhythmias in ATS1.[6] In general, focal arrhythmias have been linked to cytosolic Ca^{2+} ([Ca^{2+}]$_i$) accumulation.[8–10] Indeed, *in silico* models of ATS1 support the hypothesis that [Ca^{2+}]$_i$ accumulation underlies increased triggered activity during partial I$_{K1}$ blockade.[11,12]

Based on *ex vivo* studies in drug-induced Anderson-Tawil syndrome (DI-ATS1) models, Morita et al[6] and Poelzing and Veeraraghavan[7] proposed that arrhythmia propensity in ATS1 derives from $[Ca^{2+}]_i$ accumulation leading to increased triggered activity. However, $[Ca^{2+}]_i$ accumulation has yet to be demonstrated in an experimental model of ATS1, in part due to limitations in whole-heart $[Ca^{2+}]_i$ measurement techniques.

Although the development of ratiometric (i.e., dual wavelength) fluorescent Ca^{2+} probes has helped minimize artifacts due to inhomogeneities in fluorescence and motion, whole-heart Ca^{2+} optical mapping has lacked a calibration procedure that would satisfactorily account for multiple excitation light exposures.[13,14] Therefore, we designed and validated a ratiometric Ca^{2+} optical mapping system capable of simultaneous, quantitative, multisite measurements and use the system here to test the hypothesis that elevated $[Ca^{2+}]_i$ concomitant with APD prolongation, rather than APD dispersion, underlies arrhythmia propensity during DI-ATS1.

We demonstrate in guinea pig Langendorff-perfused ventricles that gradients of epicardial APD dispersion in DI-ATS1 were insufficient for arrhythmia induction by premature stimuli. However, APD prolongation was associated with increased incidence and severity of spontaneous and rapid pacing induced arrhythmias. Importantly, we demonstrate that this increased arrhythmia incidence is associated with significant diastolic $[Ca^{2+}]_i$ accumulation. Furthermore, APD abbreviation with the ATP-sensitive potassium channel opener pinacidil alleviated both diastolic $[Ca^{2+}]_i$ accumulation and the consequent increased arrhythmia burden.

Methods

This investigation conforms with the *Guide for the Care and Use of Laboratory Animals* published by the U.S. National Institutes of Health (NIH Publication No. 85-23, revised 1996) and was approved by the Institutional Animal Care and Use Committee of the University of Utah (Protocol No. 05-07002).

Guinea pig Langendorff preparation

Guinea pig ventricles were perfused as Langendorff preparations as previously described.[7] In brief, adult male guinea pig breeders (weight 800–1,000 g) were anesthetized with sodium pentobarbital (30 mg/kg intraperitoneally). Their hearts were rapidly excised and the atria removed and perfused as Langendorff preparations (perfusion pressure 55 mmHg) with oxygenated (100% O_2) Tyrode solution at 36.5°C of the following composition (in mmol/L): $CaCl_2$ 2, NaCl 140, KCl 4.5, dextrose 10, $MgCl_2$ 1, and HEPES 10 (pH 7.41).

Optical voltage and Ca^{2+} mapping

Ratiometric voltage optical mapping was performed as previously described[7] (see Supplemental Methods for more detail).

We developed an optical calcium mapping similar to that developed by Katra et al.[15] Ratiometric Ca^{2+} transients were determined by dividing the background-subtracted fluorescence Ca^{2+} transients at 405 nm by the background-subtracted fluorescence calcium transients at 485 nm as follows:

$$Ratio = \frac{F_{405}}{F_{485}} = \frac{\Delta F_{405} - F_{405-Background}}{\Delta F_{485} - F_{485-Background}}$$

where ΔF = actual change in fluorescent amplitude in the cameras after 405 or 485 bandpass filtering, subscript Background = light intensity without Indo-1 dye loading, and F_{405}/F_{485} = calculated ratiometric Ca^{2+} signal.

Optical action potential and $[Ca^{2+}]_i$ measurements

Motion was reduced using 7.5 mM 2,3-diacetylmonoxime. Ventricles were stimulated at 1.5 times the stimulation threshold with a unipolar silver wire placed on the basal epicardial right ventricle. *Activation time* was defined as the time of the maximum first derivative of the action potential as described previously.[16] *Repolarization* was defined as the time to 95% repolarization from peak voltage amplitude. *APD* was the time difference between activation and repolarization. APD_{50} was the time difference between activation and 50% of repolarization. *APD dispersion* was defined as the difference between epicardial regions with the longest and shortest APD (using 25 spatially contiguous optically mapped sites per region). *Relative diastolic Ca^{2+} level* and Ca^{2+} *transient amplitude* were defined as the minimum ratiometric signal before the Ca^{2+} transient upstroke and the difference between systolic and diastolic $[Ca^{2+}]_i$ values, respectively. Ca^{2+} *transient duration* was calculated from the time of 90% amplitude during systole to the time of 10% amplitude during diastole.

Drug-induced ATS1

ATS1 was modeled as described previously by perfusion of hypokalemic (2 mM KCl) Tyrode solution containing 10 μM $BaCl_2$.[7] In this report, drug-induced model of ATS1 will be referred to as DI-ATS1. Pinacidil was always perfused at 15 μM (Sigma Chemical). For most experiments, Ca^{2+} transient recordings made during control, DI-ATS1, and DI-ATS1 with pinacidil were made sequentially. In order to rule out involvement of the time-dependent component with respect to changes in Ca^{2+} transient recordings, the order of recordings in a subset of preparations was altered so that perfusion of pinacidil during DI-ATS1 directly followed control recordings.

Arrhythmia induction

After a 20-beat drive train was delivered to the anterior epicardial surface of the right ventricular base at basic cycle length (BCL) of 400 ms (previously demonstrated as the region with the longest APD),[7] an epicardial premature stimulus (S2) at the left ventricular apex (region with shortest APD)[7] was delivered through the same drive train. The S1-S2 interval was sequentially shortened by 10 ms until refractoriness was reached or an arrhythmia was induced.

Rapid pacing–induced arrhythmias were quantified at the shortest cycle length allowing for 1:1 capture. Volume-conducted electrocardiograms (ECGs) were continuously recorded in a subset of experiments in order to assess arrhythmia burden. QT intervals were corrected for changes in BCL using the formula $[QTc = QT + (1/BCL – 1)]$.[7] *Ventricular tachycardia* (VT) was defined as a run of three or more ventricular beats with a cycle length less than 250 ms. A *premature ventricular complex* (PVC) was defined as any QRS complex with different morphology that occurred less than 1.5 SD of the intrinsic cycle length. *Arrhythmia* was defined as any type of VT or PVC. *PVC frequency* was defined as the number of PVCs per minute. In order to account for interanimal variability, PVC frequency for each animal was normalized to the PVC frequency during DI-ATS1 recording.

Statistical analysis

Statistical analysis was performed with two-tailed *Student's t*-test for paired and unpaired data. Multiple regression analyses were used to characterize fluorescence Ca^{2+} signal drift both *in vitro* and in *ex vivo* preparations. Fisher exact test was used to test differences in nominal data. $P < .05$ was considered significant. All values are reported as mean ± SE unless otherwise noted.

Results

Drug induced-ATS1

A representative volume-conducted ECG shown in Figure 1A demonstrates QT-interval prolongation by approximately 60 ms during DI-ATS1 relative to control. Additionally, the T wave, which was monophasic under control conditions, was biphasic during DI-ATS1. Over all experiments, QTc during DI-ATS1 (286.7 ± 15.2 ms) was significantly longer relative to control (210.7 ± 5.2 ms, Figure 1B). Underlying the observed QTc prolongation during DI-ATS1 was APD prolongation illustrated by representative optical action potentials shown in Figure 2A. For all exper-
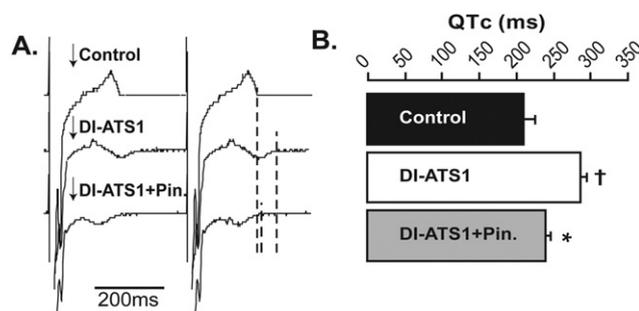
Figure 1 Volume-conducted ECG. **A:** Representative volume-conducted ECGs obtained during control **(top)**, DI-ATS1 **(middle)**, and DI-ATS1 + 15 μM pinacidil **(bottom)**. DI-ATS1 is associated with a bifurcated T wave, whereas pinacidil perfusion abolished such morphology. **B:** DI-ATS1 increased QTc compared to control (†$P < .05$, n = 6). Pinacidil (15 μM) perfusion decreased QTc compared to DI-ATS1 alone; however, it was still longer relative to control (*$P < .05$ relative to control and DI-ATS1). DI-ATS1 = drug-induced Anderson-Tawil syndrome.
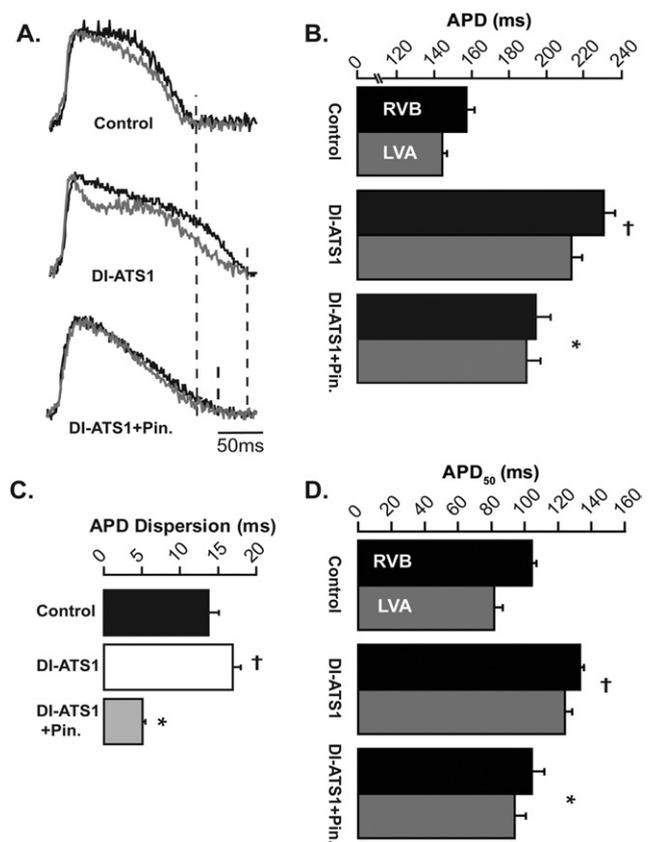
Figure 2 Drug-induced Anderson-Tawil syndrome (DI-ATS1) increases action potential duration (APD). **A:** Representative optical action potentials recorded from the same ventricular regions (RVB *black,* LVA *gray*) during control **(top)**, DI-ATS1 **(middle),** and DI-ATS1 + 15 μM pinacidil **(bottom).** DI-ATS1 prolonged APD and enhanced total APD dispersion, defined as the difference in mean APD (calculated over 25 spatially contiguous sites per region) between epicardial regions with the longest (RVB) and shortest (LVA) APD. Pinacidil (15 μM) perfusion reversed both phenomena. **B:** Mean APDs demonstrate a rise in APD during DI-ATS1 compared to control (†$P < .05$, n = 6) that was mitigated by pinacidil (15 μM) perfusion (*$P < .05$ relative to DI-ATS1 alone). However, APD after pinacidil (15 μM) perfusion remained prolonged relative to control (*$P < .05$). **C:** Total APD dispersion was greater during DI-ATS1 relative to control (†$P < .05$). Pinacidil (15 μM) perfusion decreased dispersion relative to both control and DI-ATS1 (*$P < .05$). **D:** Mean APD_{50} demonstrates a rise in APD_{50} during DI-ATS1 compared to control (†$P < .05$, n = 6) that was mitigated by pinacidil (15 μM) perfusion (*$P < .05$ relative to DI-ATS1 alone).

iments, global APD and APD_{50} were prolonged during DI-ATS1 relative to control (222.5 ± 3.5 ms vs 151.3 ± 1.3 ms, Figure 2B; and 130.1 ± 5.5 ms vs 99.8 ± 6.1 ms, Figure 2D, respectively). Additionally, APD dispersion was greater during DI-ATS1 relative to control (16.9 ± 1.0 ms vs 13.8 ± 1.3 ms, Figure 2C).

No arrhythmias (defined as one or more premature beats) were induced by premature programmed stimulation under any condition. Furthermore, VTs were neither spontaneous nor inducible under control conditions. However, during DI-ATS1, 38% of preparations experienced spontaneous VTs, and 19% experienced rapid pacing–induced VTs. Some preparations experienced one or more VT type. In total, 0% of control and 8 of 21 DI-ATS1 preparations

Table 1   Ventricular preparations exhibiting arrhythmias

Arrhythmia type	Control	DI-ATS1	DI-ATS1 + pinacidil
Programmed stimulated VT or PVC	—	0/6	0/6
Spontaneous VT	0/8	8/21*	0/16†
Rapid pacing VT	0/4	4/21	1/16
Preparations exhibiting VTs	0/8	8/21*	1/16†
PVC frequency (% of ATS1)	0.5% ± 0.3%	100%‡	20.5% ± 0.1%‡§
Arrhythmic preparations	2/8	17/17*	5/5*

Arrhythmic preparations are preparations exhibiting VTs and/or PVCs. PVC frequency was normalized to PVC frequency (no. PVCs per minute) during DI-ATS1 recording.

DI-ATS1 = drug-induced Anderson-Tawil syndrome; PVC = premature ventricular complex; VT = ventricular tachycardia.

*Fisher exact test for one-tailed probability vs control, $P < .05$.

†Fisher exact test for one-tailed probability vs DI-ATS1, $P < .05$.

‡Two-tailed Student's t-test vs control, $P < .05$.

§Two-tailed Student's t-test vs ATS1, $P < .05$.

experienced some type of VT. During DI-ATS1, all preparations experienced PVCs. PVC frequency for all experiments was normalized to the PVC frequency during DI-ATS1 (Table 1). PVC frequency during control conditions was significantly lower (by 99.5% ± 0.3%) than during DI-ATS1 alone (100%, Table 1). In total, only 2 of 8 preparations during control experienced any type of arrhythmia, all due to PVCs, relative to 17 of 17 preparations with at least one type of arrhythmia (VT and/or PVC) during DI-ATS1 (Table 1).

APD shortening during DI-ATS1 reduces frequency and duration of arrhythmias

Perfusion of pinacidil during DI-ATS1 (DI-ATS1+Pinacidil) shortened QTc to near control values as demonstrated by a representative trace in Figure 1A (right). Over all experiments, pinacidil shortened QTc relative to DI-ATS1 (Figure 1B); however, QTc was still prolonged (240.8 ± 5.8 ms, Figure 1B) relative to control. QT shortening during DI-ATS1+Pinacidil was associated with an abbreviation of APD relative to DI-ATS1 alone (Figure 2A). Specifically, DI-ATS1+Pinacidil significantly shortened APD to 190.6 ± 3.7 ms (Figure 2B), which was significantly greater relative to control. Additionally, DI-ATS1+Pinacidil significantly shortened APD$_{50}$ to 99.5 ± 6.1 ms (Figure 2D), which was not significantly different from control. Finally, DI-ATS1+Pinacidil reduced APD dispersion to 5.0 ± 0.4 ms (Figure 2C), which was significantly lower than during control or DI-ATS1 alone.

DI-ATS1+Pinacidil abolished spontaneous VTs, but the incidence of rapid pacing–induced VTs was not significantly reduced (6%, Table 1). Importantly, DI-ATS1+Pinacidil significantly reduced PVC frequency by 79.5% ± 0.1% relative to DI-ATS1 alone (Table 1), which was significantly greater relative to control (0.5% ± 0.3%). Finally, ECG was continuously monitored in a subset of DI-ATS1+Pinacidil preparations (n = 5). In this group, all preparations exhibited some form of arrhythmia (VT and/or PVC), which was not significantly different from DI-ATS1 but was significantly greater than control.

Validation of ratiometric [Ca^{2+}]$_i$ mapping

In order to quantify relative changes in [Ca^{2+}]$_i$ during ATS1, it was important to validate Ca^{2+} independent drift. The F_{405}/F_{485} drift was measured *in vitro* (see Supplemental Results) and *ex vivo* in Langendorff-perfused guinea pig ventricles (n = 3), where recordings were made every 5 minutes for 1 hour. Ca^{2+} transients recorded from the same epicardial site at different exposure times demonstrate an upward shift in signal consistent with *in vitro* observations (Figure 3A, Exp1 *black,* first exposure; Exp13 *gray,* last exposure). Both diastolic [Ca^{2+}]$_i$ and Ca^{2+} transient amplitude were significantly higher during Exp13 relative to Exp1 (Figure 3E). Multiple regression analysis revealed a significant correlation of observed drift with cumulative exposure (parameterized as number of exposures). Specifically, diastolic [Ca^{2+}]$_i$ increased at a rate of 3.77% (95% confidence interval 3.37–4.17, R^2 = 0.79) per exposure (Figure 3B). Importantly, Ca^{2+} transient duration (Figure 4A), QRS duration, and QT interval (see Supplemental Figure 2) were unaffected by the number of exposures.

Mathematically correcting measured transients by subtracting 3.77% per exposure from the ratiometric fluorescence Ca^{2+} signal resulted in a high degree of morphologic correspondence between Ca^{2+} transients recorded several exposures apart (Figure 3C). Over all experiments, mathematical drift correction returned Ca^{2+} transient amplitude and diastolic [Ca^{2+}]$_i$ after 13 exposures to Exp1 levels (Figures 3D and 3E).

Validation of Ca^{2+} drift correction

Under control conditions, rapid pacing (BCL = 200 ms, Exp2, Figure 4) significantly increased drift-corrected diastolic [Ca^{2+}]$_i$ by 7.6% ± 1.4% (n = 3) relative to baseline pacing (BCL = 400 ms, Exp1) as demonstrated by representative data shown in Figure 4A. Cessation of rapid pacing (BCL = 400, Exp3) returned drift corrected diastolic [Ca^{2+}]$_i$ to values similar to baseline (BCL = 400, Exp1, 6.7% ± 0.9% decrease). To further validate our ability to measure changes in diastolic [Ca^{2+}]$_i$, we inhibited SERCA2a with 5 μM cyclopiazonic acid, which significantly increased drift-corrected diastolic [Ca^{2+}]$_i$ by 15.2% ± 1.5%
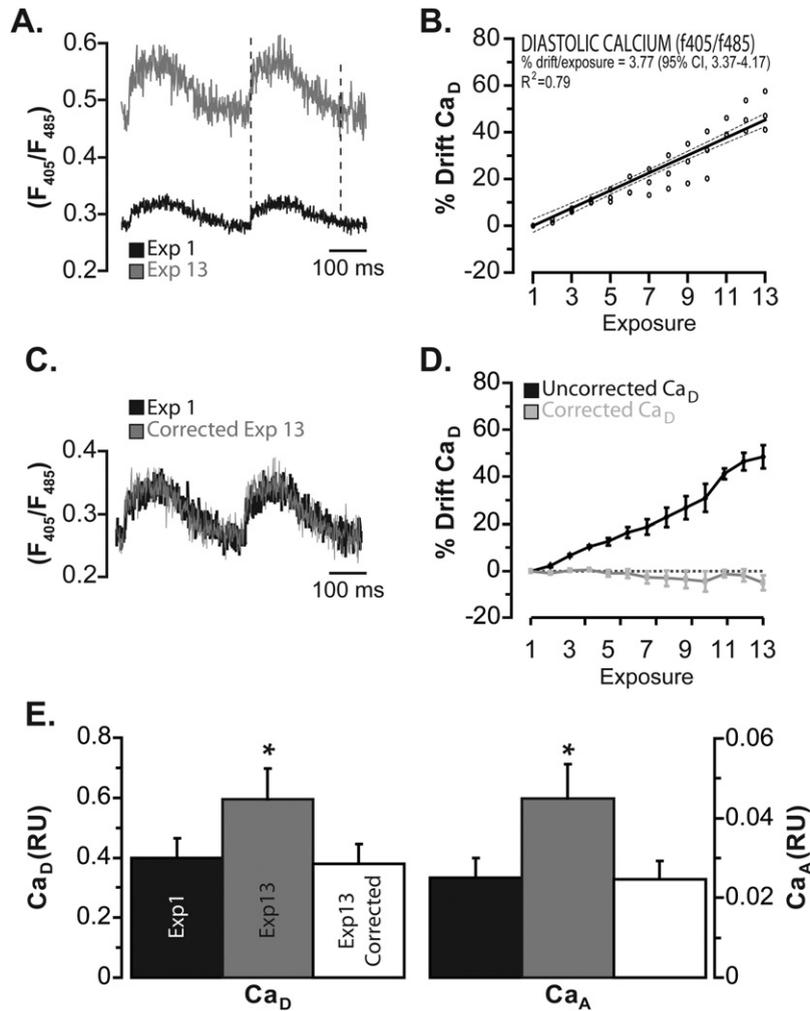
Figure 3 *Ex vivo* characterization of Ca^{2+} drift. **A:** Representative ratiometric Ca^{2+} transients (Exp1 *black,* Exp13 *gray*) recorded during repeated exposures to excitation light at 5-minute intervals. The 13th exposure (Exp13) exhibited an upward shift of Ca^{2+} transients relative to the first recording (Exp1). **B:** Multiple regression analysis of diastolic $[Ca^{2+}]_i$ (Ca_D) drift (n = 3) revealed a significant correlation between drift and number of exposures. Drift = 3.77% (95% confidence interval 3.37–4.17, R^2 = 0.79) increase in Ca_D per exposure. **C:** Representative Ca^{2+} transients from Exp1 *(black)* and drift-corrected Ca^{2+} transients from Exp13 *(gray).* Subtraction of Ca_D drift leads to high degree of morphologic correspondence between Ca^{2+} transients recorded several exposures apart. **D:** Pooled Ca_D data depicting percent Ca_D drift per exposure *(black).* Correction for observed drift leads to no change in Ca_D *(gray). Dotted gray line* marks zero level. **E:** Summary data for all experiments depicting changes in Ca_D **(left)** and Ca^{2+} transient amplitude (Ca_A) **(right)** secondary to exposure. During the last recording (Exp13), both Ca_D and Ca_A rose significantly (*P <.05 vs Exp1). Drift correction returned both parameters to baseline.

(n = 3) relative to control as demonstrated by representative data shown in Figure 4B. All subsequent $[Ca^{2+}]_i$ measurements were therefore corrected for drift. In order to compare relative changes between different experiments, the offset of diastolic $[Ca^{2+}]_i$ was normalized to the offset of diastolic $[Ca^{2+}]_i$ in the first recording of each experiment.

DI-ATS1 alters $[Ca^{2+}]$ handling

Representative Ca^{2+} transients shown in Figure 5A demonstrate that DI-ATS1 shifts ratiometric Ca^{2+} transients upward. Diastolic $[Ca^{2+}]_i$ during DI-ATS1 was significantly greater relative to control by 17.9% ± 1.8% (n = 10, Figure 5B). Additionally, DI-ATS1 significantly elevated Ca^{2+} transient amplitude by 18.1% ± 1.3% relative to control (Figures 5A and 5B). Perfusion of pinacidil (15 μM) during DI-ATS1 attenuated the upward shift in diastolic $[Ca^{2+}]_i$ (Figure 5A). This effect was observed irrespective of the exper-

imental order. For all experiments, DI-ATS1+Pinacidil reduced diastolic $[Ca^{2+}]_i$ by 12.7% ± 1.7% (Figure 5C) relative to DI-ATS1 alone; however, diastolic $[Ca^{2+}]_i$ remained significantly greater relative to control (6.5% ± 2.2%). Furthermore, pinacidil did not reverse the rise in Ca^{2+} transient amplitude (Figures 5B and 5C). Specifically, Ca^{2+} transient amplitude during DI-ATS1 was not significantly different after pinacidil perfusion; therefore, Ca^{2+} transient amplitude during DI-ATS1+Pinacidil remained significantly greater relative to control (19.4% ± 2.3%).

Discussion

Several studies hypothesized that $[Ca^{2+}]_i$ accumulation concomitant with APD prolongation underlies arrhythmias in ATS1[11,17] and DI-ATS1.[6,7] However, $[Ca^{2+}]_i$ accumulation had not been demonstrated in whole-heart preparations in part because of methodologic difficulties in quantitative
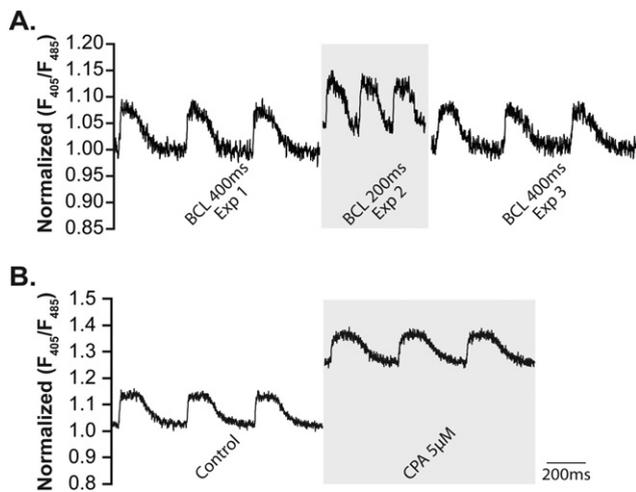
Figure 4   *Ex vivo* validation of Ca^{2+} drift correction. **A:** Representative drift-corrected Ca^{2+} transients during baseline pacing at basic cycle length (BCL) 400 ms **(left),** followed by rapid pacing at BCL 200 and subsequent return to baseline pacing. Diastolic [Ca^{2+}]$_i$ (Ca$_D$) after mathematical correction were normalized to Ca$_D$ in the first recording. Rapid pacing significantly increased Ca$_D$, whereas a return to baseline pacing reversed the rise in Ca$_D$. **B:** Representative drift-corrected Ca^{2+} transients recorded during control **(left),** followed by 5 μM cyclopiazonic acid (CPA) perfusion. CPA perfusion significantly increased Ca$_D$.

[Ca^{2+}]$_i$ measurement using ratiometric Ca^{2+} optical mapping. In this study, we demonstrate that DI-ATS1 was associated with [Ca^{2+}]$_i$ accumulation concomitant with APD prolongation. Attenuating [Ca^{2+}]$_i$ accumulation during DI-ATS1 and reducing APD significantly reduced spontaneous VTs and PVC frequency. Furthermore, programmed electrical stimulation failed to induce arrhythmias despite increased APD dispersion during DI-ATS1. However, these data suggest that APD prolongation in DI-ATS1 is associated with [Ca^{2+}]$_i$ accumulation, which subsequently is associated with increased arrhythmogenic burden in ATS1.

APD and arrhythmias in DI-ATS1

The ECG features observed in our DI-ATS1 model were consistent with previous experimental studies[6,7] as well as clinical observations:[2] The QT interval prolonged on the volume-conducted ECG and a double repolarization wave that was observed during DI-ATS was not present during control (Figure 1A). QT-interval prolongation was associated with APD prolongation quantified from the anterior epicardial surface of guinea pig myocardium (Figure 2A), which is consistent with previous experimental and *in silico* studies of ATS1.[5–7,11,17]

APD prolonged heterogeneously in DI-ATS1, resulting in increased interventricular APD gradients relative to control. Despite the larger APD gradients, programmed electrical stimulation failed to induce an arrhythmia in any of the hearts tested in this study. This finding suggests that APD dispersion may have been of insufficient magnitude to precipitate reentrant arrhythmias.[18,19] Successful arrhythmia induction by programmed electrical stimulation previously

reported in a guinea pig model of LQT3 suggests that occurrence of reentry is not precluded by the size of the guinea pig heart.[20] Furthermore, that study reported a significantly larger APD dispersion than observed in our model, lending credence to the hypothesis of insufficient dispersion of repolarization for reentry to occur in our model. Therefore, our data argue against involvement of dispersion of repolarization in arrhythmogenesis in our model but do not completely rule out its involvement. Furthermore, it is important to note that the methodologies used in the present study preclude the assessment of transmural dispersion of repolarization. However, Tsuboi and Antzelevitch[5] concluded that transmural dispersion of repolarization gradients were insufficient for arrhythmia induction by programmed electrical stimulation in a canine left ventricular wedge model of DI-ATS1. Taken together, these data still suggest that the degree of dispersion observed in DI-ATS1 likely was insufficient for reentrant arrhythmia induction.

In order to test the effects of APD abbreviation on the DI-ATS1 phenotype, we perfused pinacidil, an ATP-sensitive potassium channel opener. Pinacidil decreased APD gradients in DI-ATS1 below those observed in DI-ATS1 alone or in control and reduced the incidence of arrhythmias but did not abolish them. Specifically, PVC frequency, a marker of arrhythmia vulnerability,[21,22] during
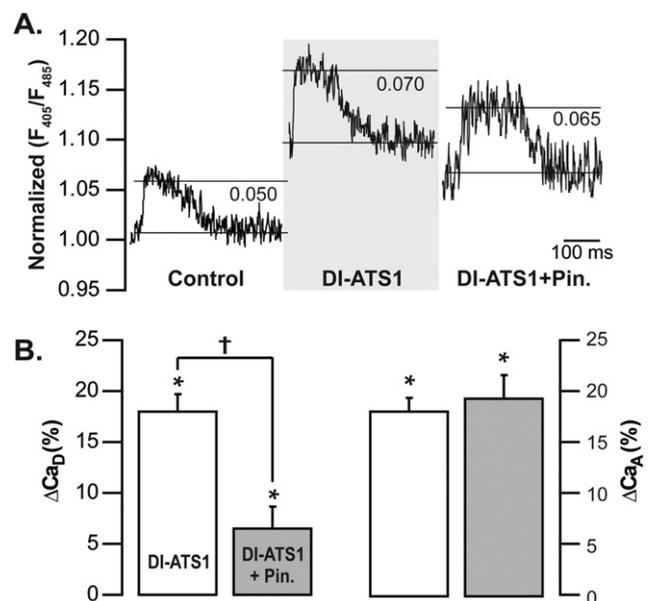
Figure 5   Drug-induced Anderson-Tawil syndrome (DI-ATS1) alters [Ca^{2+}] handling. **A:** Representative drift-corrected Ca^{2+} transients recorded during control, DI-ATS1, and DI-ATS1 + 15 μM pinacidil perfusion. During DI-ATS1, Ca^{2+} transients were shifted upward, whereas pinacidil partially reversed that shift. Both DI-ATS1 and DI-ATS1 + pinacidil exhibit greater Ca^{2+} transient amplitude (Ca$_A$) *(horizontal lines)* relative to control. **B:** Summary of ΔCa$_D$ **(left)** and ΔCa$_A$ **(right)** relative to control. DI-ATS1 significantly increased Ca$_D$ and Ca$_A$ relative to control (*P <.05, n = 10). Pinacidil perfusion (15 μM) decreased Ca$_D$ relative to DI-ATS1 alone (†P <.05). Pinacidil did not completely revert Ca$_D$ to control levels (*P <.05). Pinacidil had no effect on Ca$_A$ relative to DI-ATS1 alone.

pinacidil perfusion was lower relative to DI-ATS1 but still was higher relative to control. Therefore, these data suggest that gradients of repolarization in DI-ATS1 are unlikely to be a significant substrate for arrhythmias in this condition.

On the other hand, pinacidil attenuated the rise in APD_{50} due to DI-ATS1 such that APD_{50} during control and DI-ATS1+Pinacidil were not significantly different. Therefore, the observation that arrhythmias were reduced but still present during DI-ATS1+Pinacidil further suggests that these arrhythmias are not correlated to APD_{50} or action potential plateau prolongation.

The two conditions of DI-ATS1 and DI-ATS1+Pinacidil exhibited final repolarization (APD) prolongation and $[Ca^{2+}]_i$ accumulation relative to control. These findings suggest two mechanisms that may not necessarily be independent. Specifically, prolongation of final repolarization, as estimated by APD, could also be a substrate for increased triggered activity in DI-ATS1. The hypothesis that APD prolongation leads to recovery from inactivation of L-type calcium channels is not well supported by changes in APD_{50} but could be supported by total APD prolongation. However, it is well established that APD prolongation can increase $[Ca^{2+}]_i$ accumulation.[10] Therefore, triggered activity observed in our DI-ATS1 model still suggests a prominent but not necessarily exclusive role for $[Ca^{2+}]_i$ accumulation as an arrhythmia mechanism in DI-ATS1.

Proposed arrhythmia mechanism in ATS1

Arrhythmias in ATS1 patients are often preceded by a high PVC incidence, presumably due to triggered activity, and PVC burden in ATS1 is exacerbated by hypokalemia.[3,23] Importantly, it has been demonstrated that hypokalemia alone leads to $[Ca^{2+}]_i$ accumulation and the increased incidence of arrhythmias.[24] Based on these findings, the following mechanism of increased incidence of arrhythmias has been proposed. $[Ca^{2+}]_i$ accumulation is associated with increased sarcoplasmic reticular Ca^{2+} loading and an increased propensity for triggered activity, presumably due to spontaneous Ca^{2+} release from the sarcoplasmic reticulum.[25] The resultant spontaneous Ca^{2+} release may lead to depolarization via transient inward currents carried by the forward mode Na^+/Ca^{2+} exchanger, facilitating triggered activity.[8–10] This leads to the hypothesis that $[Ca^{2+}]_i$ accumulation, secondary to hypokalemia, underlies triggered activity in ATS1 or DI-ATS1.[6,7]

Sung et al[11] tested this hypothesis in an *in silico* study and suggested a role for abnormal $[Ca^{2+}]_i$ cycling in ATS1-associated arrhythmias. This finding was indirectly affirmed by Morita et al,[6] who reported that Ca^{2+} channel blockade by verapamil abolished all arrhythmic activity in a canine left ventricular wedge model of DI-ATS1. However, $[Ca^{2+}]_i$ accumulation during DI-ATS1 has not been previously demonstrated in an *ex vivo* intact ventricular model.

Validation of ratiometric calcium mapping

In order to assess the effects of DI-ATS1 on $[Ca^{2+}]_i$ handling, it is important to characterize any Ca^{2+}-independent changes in Indo-1 fluorescence. Despite previous calibration attempts,[26] many reports indicated that incomplete de-esterification of Indo-1/AM along with excitation intensity–dependent photobleaching of Indo-1 affect ratiometric fluorescent Ca^{2+} measurement.[27–30] Specifically, the fluorescent signals corresponding to bound and unbound Indo-1 (F_{405} and F_{485}, respectively) drift toward zero at two different rates, resulting in an apparent decrease in the ratiometric Ca^{2+} signal.[28] In our experimental setup, individual fluorescent Ca^{2+} signals (F_{405} and F_{485}) also decreased, yet the ratiometric Ca^{2+} increased (see Supplemental Figure 1A). These seemingly contradictory findings could be attributed to the following experimental differences: the choices of dye of Indo-1 versus ester form of Indo-1 (Indo-1/AM), emission filters, and/or photodetector spectral response. The relative drift rates of the F_{405} and F_{485} signals will dictate whether the ratiometric signal drifts upward or downward.

Future studies that measure $[Ca^{2+}]_i$ over time should validate $[Ca^{2+}]_i$ response as a function of exposure.[28,30] The absence of concomitant changes in ECG parameters or Ca^{2+} transient duration (see Supplemental Figure 2) suggests that these changes in fluorescent Ca^{2+} signals may be dye related rather than physiologic in origin. Importantly, mathematical correction of ratiometric fluorescent Ca^{2+} transients by subtracting the observed drift from the signal resulted in a high degree of morphologic correspondence between ratiometric transients recorded several exposures apart (Figure 3C). Finally, the optically measured, drift-corrected diastolic $[Ca^{2+}]_i$ increased during rapid pacing and returned to baseline upon cessation of rapid pacing (Figure 4A), which is consistent with previous studies.[22,31] Likewise, SERCA2a inhibition by 5 μM cyclopiazonic acid perfusion led to $[Ca^{2+}]_i$ accumulation, as previously demonstrated.[32] Therefore, this mathematical drift correction was applied to all subsequent recordings.

DI-ATS1 alters $[Ca^{2+}]_i$ handling

DI-ATS1 was associated with a significant rise in $[Ca^{2+}]_i$ as reflected in both diastolic $[Ca^{2+}]_i$ and Ca^{2+} transient amplitude and an increased incidence of ventricular arrhythmias. These data are the first direct evidence in an intact ventricular preparation for $[Ca^{2+}]_i$ accumulation during DI-ATS1. Furthermore, these data are consistent with the theoretical mechanisms proposed for arrhythmias in ATS1.[6,7,11] More generally, the finding that $[Ca^{2+}]_i$ accumulation concomitant with APD prolongation is related to increased arrhythmia propensity is consistent with previous studies using alternative methods of $[Ca^{2+}]_i$ loading to increase the incidence of triggered activity.[8–10,21,22] Further studies are necessary to elucidate the relationship among the extent of $[Ca^{2+}]_i$ accumulation, APD prolongation, and the origin of triggered activity during DI-ATS1.

Study limitations

Although APD gradients in guinea pig (present study) or canine[5] were not associated with increased arrhythmia propensity, APD distribution and heterogeneity are know to vary among animal models.[33,34] The nature of electrophysiologic remodeling induced by chronic functional I_{K1} down-regulation, as occurs in patients with ATS1, remains unclear.[5–7,11,17] Furthermore, it is well appreciated that pharmacologic models of cardiac disease should be interpreted cautiously due to the acute nature of the study as well as the specificity of the intervention.[35]

Conclusion

This study suggests that arrhythmias during DI-ATS1 may be the result of triggered activity secondary to prolonged APD and altered $[Ca^{2+}]_i$ cycling and less likely dependent on large gradients of repolarization acting as a substrate for reentrant arrhythmias. Therefore, ameliorating myocyte $[Ca^{2+}]_i$ load may prove a more effective therapeutic goal in ATS1 compared to decreasing APD gradients.
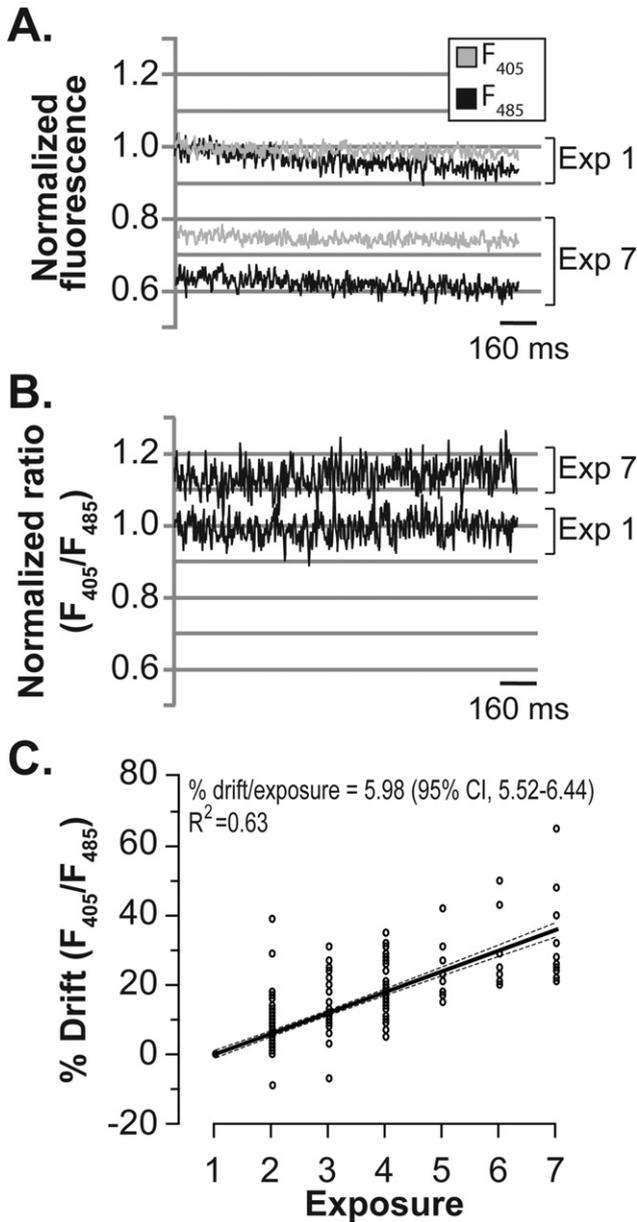
Appendix

Supplementary data

Supplementary data associated with this article can be found, in the online version, at doi:10.1016/j.hrthm.2010.03.044.
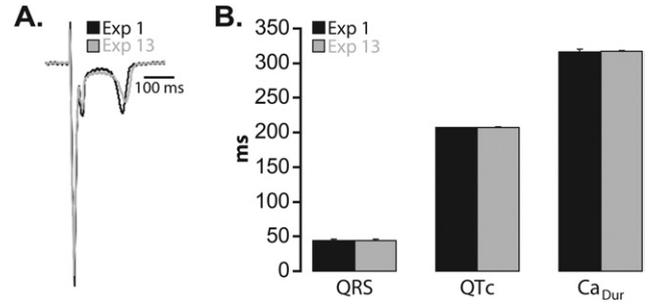
References

1. Plaster NM, Tawil R, Tristani-Firouzi M, et al. Mutations in Kir2.1 cause the developmental and episodic electrical phenotypes of Andersen's syndrome. Cell 2001;105:511–519.
2. Tristani-Firouzi M, Jensen JL, Donaldson MR, et al. Functional and clinical characterization of KCNJ2 mutations associated with LQT7 (Andersen syndrome). J Clin Invest 2002;110:381–388.
3. Tawil R, Ptacek LJ, Pavlakis SG, et al. Andersen's syndrome: potassium-sensitive periodic paralysis, ventricular ectopy, and dysmorphic features. Ann Neurol 1994;35:326–330.
4. Zhang L, Benson DW, Tristani-Firouzi M, et al. Electrocardiographic features in Andersen-Tawil syndrome patients with KCNJ2 mutations: characteristic T-U-wave patterns predict the KCNJ2 genotype. Circulation 2005;111:2720–2726.
5. Tsuboi M, Antzelevitch C. Cellular basis for electrocardiographic and arrhythmic manifestations of Andersen-Tawil syndrome (LQT7). Heart Rhythm 2006;3:328–335.
6. Morita H, Zipes DP, Morita ST, Wu J. Mechanism of U wave and polymorphic ventricular tachycardia in a canine tissue model of Andersen-Tawil syndrome. Cardiovasc Res 2007;75:510–518.
7. Poelzing S, Veeraraghavan R. Heterogeneous ventricular chamber response to hypokalemia and inward rectifier potassium channel blockade underlies bifurcated T wave in guinea pig. Am J Physiol Heart Circ Physiol 2007;292:H3043–H3051.
8. Marban E, Robinson SW, Wier WG. Mechanisms of arrhythmogenic delayed and early afterdepolarizations in ferret ventricular muscle. J Clin Invest 1986;78:1185–1192.
9. Nuss HB, Kaab S, Kass DA, Tomaselli GF, Marban E. Cellular basis of ventricular arrhythmias and abnormal automaticity in heart failure. Am J Physiol 1999;277:H80–H91.
10. Volders PG, Vos MA, Szabo B, et al. Progress in the understanding of cardiac early afterdepolarizations and torsades de pointes: time to revise current concepts. Cardiovasc Res 2000;46:376–392.
11. Sung RJ, Wu SN, Wu JS, Chang HD, Luo CH. Electrophysiological mechanisms of ventricular arrhythmias in relation to Andersen-Tawil syndrome under conditions of reduced I_{K1}: a simulation study. Am J Physiol Heart Circ Physiol 2006;291:H2597–H2605.
12. Silva J, Rudy Y. Mechanism of pacemaking in I(K1)-downregulated myocytes. Circ Res 2003;92:261–263.
13. Brandes R, Figueredo VM, Camacho SA, Massie BM, Weiner MW. Suppression of motion artifacts in fluorescence spectroscopy of perfused hearts. Am J Physiol 1992;263:H972–H980.
14. Kong W, Walcott GP, Smith WM, Johnson PL, Knisley SB. Emission ratiometry for simultaneous calcium and action potential measurements with coloaded dyes in rabbit hearts: reduction of motion and drift. J Cardiovasc Electrophysiol 2003;14:76–82.
15. Katra RP, Pruvot E, Laurita KR. Intracellular calcium handling heterogeneities in intact guinea pig hearts. Am J Physiol Heart Circ Physiol 2004;286:H648–H656.
16. Girouard SD, Pastore JM, Laurita KR, Gregory KW, Rosenbaum DS. Optical mapping in a new guinea pig model of ventricular tachycardia reveals mechanisms for multiple wavelengths in a single reentrant circuit. Circulation 1996;93:603–613.
17. Seemann G, Sachse FB, Weiss DL, Ptacek LJ, Tristani-Firouzi M. Modeling of I_{K1} mutations in human left ventricular myocytes and tissue. Am J Physiol Heart Circ Physiol 2007;292:H549–H559.
18. Akar FG, Rosenbaum DS. Transmural electrophysiological heterogeneities underlying arrhythmogenesis in heart failure. Circ Res 2003;93:638–645.
19. Coronel R, Wilms-Schopman FJ, Opthof T, Janse MJ. Dispersion of repolarization and arrhythmogenesis. Heart Rhythm 2009;6:537–543.
20. Restivo M, Caref EB, Kozhevnikov DO, El-Sherif N. Spatial dispersion of repolarization is a key factor in the arrhythmogenicity of long QT syndrome. J Cardiovasc Electrophysiol 2004;15:323–331.
21. Laurita KR, Katra RP. Delayed after depolarization-mediated triggered activity associated with slow calcium sequestration near the endocardium. J Cardiovasc Electrophysiol 2005;16:418–424.
22. Katra RP, Laurita KR. Cellular mechanism of calcium-mediated triggered activity in the heart. Circ Res 2005;96:535–542.
23. Nichols CG, Makhina EN, Pearson WL, Sha Q, Lopatin AN. Inward rectification and implications for cardiac excitability. Circ Res 1996;78:1–7.
24. Tribulova N, Manoach M, Varon D, Okruhlicova L, Zinman T, Shainberg A. Dispersion of cell-to-cell uncoupling precedes low K^+-induced ventricular fibrillation. Physiol Res 2001;50:247–259.
25. Diaz ME, Trafford AW, O'Neill SC, Eisner DA. Measurement of sarcoplasmic reticulum Ca^{2+} content and sarcolemmal Ca^{2+} fluxes in isolated rat ventricular myocytes during spontaneous Ca^{2+} release. J Physiol 1997;501(Pt 1):3–16.
26. Brandes R, Figueredo VM, Camacho SA, Baker AJ, Weiner MW. Quantitation of cytosolic $[Ca^{2+}]$ in whole perfused rat hearts using Indo-1 fluorimetry. Biophys J 1993;65:1973–1982.
27. Wahl M, Lucherini MJ, Gruenstein E. Intracellular Ca^{2+} measurement with Indo-1 in substrate-attached cells: advantages and special considerations. Cell Calcium 1990;11:487–500.
28. Scheenen WJ, Makings LR, Gross LR, Pozzan T, Tsien RY. Photodegradation of indo-1 and its effect on apparent Ca^{2+} concentrations. Chem Biol 1996;3:765–774.
29. Luckhoff A. Measuring cytosolic free calcium concentration in endothelial cells with indo-1: the pitfall of using the ratio of two fluorescence intensities recorded at different wavelengths. Cell Calcium 1986;7:233–248.
30. Lee HC, Mohabir R, Smith N, Franz MR, Clusin WT. Effect of ischemia on calcium-dependent fluorescence transients in rabbit hearts containing indo 1. Correlation with monophasic action potentials and contraction. Circulation 1988;78:1047–1059.
31. Laurita KR, Katra R, Wible B, Wan X, Koo MH. Transmural heterogeneity of calcium handling in canine. Circ Res 2003;92:668–675.
32. Abe F, Karaki H, Endoh M. Effects of cyclopiazonic acid and ryanodine on cytosolic calcium and contraction in vascular smooth muscle. Br J Pharmacol 1996;118:1711–1716.
33. Liu DW, Antzelevitch C. Characteristics of the delayed rectifier current (I_{Kr} and I_{Ks}) in canine ventricular epicardial, midmyocardial, and endocardial myocytes. A weaker I_{Ks} contributes to the longer action potential of the M cell. Circ Res 1995;76:351–365.
34. Warren M, Guha PK, Berenfeld O, et al. Blockade of the inward rectifying potassium current terminates ventricular fibrillation in the guinea pig heart. J Cardiovasc Electrophysiol 2003;14:621–631.
35. Baker LC, Wolk R, Choi BR, et al. Effects of mechanical uncouplers, diacetyl monoxime, and cytochalasin-D on the electrophysiology of perfused mouse hearts. Am J Physiol Heart Circ Physiol 2004;287:H1771–H1779.

A.

B.

C.

A.

B.

Supplemental Figure 2 Effect of time on Ca$_{Dur}$ and ECG parameters

A) Representative volume-conducted ECGs recorded under control conditions to assess Ca^{2+}-independent changes in indo-1 fluorescence. No changes in the ECG morphology were observed between the first (Exp 1 – black) and last recordings (Exp 13 – grey). **B)** Summary data (n = 3) depicting no significant difference in QRS, QT$_c$, and Ca^{2+} transients duration (Ca$_{Dur}$) between the first (Exp 1 – black) and last recordings (Exp 13 – grey).

Supplemental Figure 1 *In Vitro* Characterization of Ca^{2+} Fluorescence Drift

A) Representative fluorescent Ca^{2+} signals (gray – F$_{405}$, black – F$_{485}$) of a vial containing 0.1 μM [Ca^{2+}] and 0.1 μM Indo-1 during the first (Exp 1) and last exposures (Exp 7). In this example during Exp 1, F$_{485}$ decreased faster relative to F$_{405}$ (−0.080% [95% CI, −0.085 – −0.075] per second vs −0.024% [95% CI, −0.027 – −0.020] per second, respectively). After 7 exposures (Exp 7), both F$_{405}$ and F$_{485}$ decreased relative to the first recording (Exp 1). **B)** Representative ratiometric fluorescent Ca^{2+} signals corresponding to the F$_{405}$ and F$_{485}$ in Figure 3A. The drift in F$_{405}$ and F$_{485}$ during Exp 1 translated into a rise in F$_{405}$/F$_{485}$ within the recording (0.023% [95% CI, 0.006 – 0.039] per 1 second). After 7 exposures (Exp 7) ratiometric fluorescent Ca^{2+} signals was enhanced relative to Exp 1. **C)** Multiple regression analysis of drift measurements pooled from all experiments (n = 57) conducted at different exposure frequencies. The drift demonstrated a significant correlation with the number of exposures with rate of 5.98% ([95% CI 5.52–6.44], R^2 = 0.63) increase in ratiometric Ca^{2+} fluorescence per exposure.